Optimal Phasing for Parallel Transmission Lines to Minimize AC Interference

Arash Tavighi Hamed Ahmadi Mažana Armstrong José R. Martí

***Abstract*—AC interference is a growing concern within the power industry due to the proximity of other utilities (pipelines, railways, etc.) sharing the same right-of-way (ROW) and corresponding safety issues. This paper presents a methodology for determining the optimal phasing of power transmission lines to reduce the interference and improve on safe operation of utilities sharing the same ROW. The induced voltage levels on an adjacent conductor are calculated using various existing methods to compare their accuracy. Several important findings are reported here regarding the AC interference modeling under steady-state condition. The importance of the inherent unbalance in phase currents and the effect of soil resistivity are discussed in detail. The test case in the study is based on a project in BC Hydro to build two 500 kV transmission lines located in the Peace Region area, British Columbia. The results of this study were used in determining the optimal phasing for these transmission lines.**

***Index Terms*—AC interference, phase arrangement.**

I. Introduction

Due to the environmental and regulatory restrictions, utilities often share the same corridor: power transmission lines, oil and gas pipelines, railways, etc. The electromagnetic coupling between the overhead transmission lines and adjacent metallic conductors induces a voltage that can be a safety hazard for workers and the public. Under normal operation, the induced voltages can result in gradual damage to the coating of pipelines, corrosion of the metallic surface, and eventually mechanical breakdown of the pipelines. This situation can be worse for transient conditions, when a fault occurs in the system which, in turn, causes larger induced voltages. Above-ground pipelines are more at risk of transient-induced voltages than buried pipelines [1].

BC Hydro is planning to build two 500 kV lines in the Peace Region area in British Columbia. This area is frequented by pipelines, railways, and farm fences. For this reason, minimizing the AC interference from the new transmission lines on the adjacent objects is crucial.

There are various methods for reducing the induced voltages to acceptable levels. One option is to maintain a safe distance between transmission lines and a parallel conductor [1] which calls for acquiring permits from various municipalities. Other mitigation strategies are shielding the conductors of overhead transmission lines [2], strengthening the pipelines coating [3], or installing appropriate grounding for the victim conductor, which can be costly. One of the effective methods is the optimal phasing of energized conductors. The effect of phase arrangement on the electric and magnetic fields around a double-circuit transmission lines was analyzed in [4]. In this paper, the option of optimal phasing is chosen to minimize the induced voltage from energized transmission lines to an adjacent victim conductor. The impacts of the inherent unbalance in the phase currents [5], soil resistivity, separation distance of the victim conductor, and configuration of transmission lines are studied.

Several simulation tools have been developed for electromagnetic AC interference studies [6]–[8]. Some of the numerical implementations are based on the Electro-Magnetic Transients Programs (EMTP) [9][10]. Although the main application of EMTP is for transient studies, these tools can also be used for steady-state analysis [11]. In this paper, Voltage Drop Equations (VDE) is used for the calculation of induced voltage. The results obtained using VDE are compared with EMTP simulation using the Universal Line Model (ULM) [12] and the Discrete Time Fourier Series (DTFS) [13].

II. Voltage Drop Equations (VDE) to Calculate the Induced Voltage on a Victim Conductor

To derive Voltage Drop Equations (VDE), let us assume a simple case of two transmission lines in parallel with a victim conductor for a length Δx as shown in Fig. 1.

The adjacent conductor is shorted at the sending-end and is open at the receiving-end. Since no current passes through this conductor, the induced voltage at the receiving-end is due to the AC interference from the energized lines. In this case, VDE can be written as

$$\Delta \mathbf{V}_{xy} = \mathbf{V}_x - \mathbf{V}_y = \mathbf{Z}\mathbf{I}\Delta x \tag{1}$$

In (1), Carson's formula [14] is used for the calculation of the impedance matrix $\mathbf{Z}$. Equation (1) can be written in a matrix form by separating the victim conductor "p" from the transmission lines "ℓ"

$$\Delta \mathbf{V}_{xy} = \begin{bmatrix} \mathbf{V}_{\ell x} \\ 0 \end{bmatrix} - \begin{bmatrix} \mathbf{V}_{\ell y} \\ \mathbf{V}_{py} \end{bmatrix} = \begin{bmatrix} \mathbf{Z}_{\ell\ell} & \mathbf{Z}_{\ell p} \\ \mathbf{Z}_{p\ell} & \mathbf{Z}_{pp} \end{bmatrix} \begin{bmatrix} \mathbf{I}_{\ell} \\ 0 \end{bmatrix} \Delta x \tag{2}$$

For the case of current source energization, the branch currents $\mathbf{I}_\ell$ are known. The induced voltage on the victim conductor $\mathbf{V}_{py}$ can be calculated as

$$\mathbf{V}_{py} = -\mathbf{Z}_{p\ell}\mathbf{I}_\ell \Delta x \tag{3}$$

Arash Tavighi and José R. Martí are with the Department of Electrical and Computer Engineering, University of British Columbia (UBC), 2332 Main Mall, Vancouver, BC, V6T 1Z4, Canada (emails: arashtav@ece.ubc.ca, jrms@ece.ubc.ca). Hamed Ahmadi and Mažana Armstrong are with the Transmission Line Electrical Design, BC Hydro, 6911 Southpoint Drive, E07, Burnaby, BC, V3N 4X8 (emails: hamed.ahmadi@bchydro.com, and mazana.armstrong@bchydro.com).

978-1-5386-2410-4/18/$31.00 ©2018 IEEE

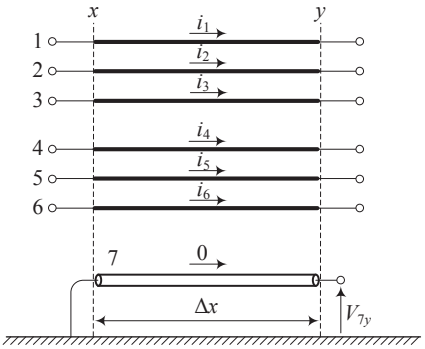

Fig. 1. Two transmission lines in parallel with a victim conductor.

For the case of voltage source energization, the branch currents $\mathbf{I}_\ell$ are unknown. To calculate the induced voltage for this condition, (2) can be re-written as

$$\begin{bmatrix}\mathbf{I}_\ell \\ 0\end{bmatrix} = \begin{bmatrix}\mathbf{Y}_{\ell\ell} & \mathbf{Y}_{\ell p} \\ \mathbf{Y}_{p\ell} & \mathbf{Y}_{pp}\end{bmatrix} \begin{bmatrix}\mathbf{V}_{\ell x} - \mathbf{V}_{\ell y} \\ -\mathbf{V}_{py}\end{bmatrix} \Delta x \tag{4}$$

where

$$\begin{bmatrix}\mathbf{Y}_{\ell\ell} & \mathbf{Y}_{\ell p} \\ \mathbf{Y}_{p\ell} & \mathbf{Y}_{pp}\end{bmatrix} = \begin{bmatrix}\mathbf{Z}_{\ell\ell} & \mathbf{Z}_{\ell p} \\ \mathbf{Z}_{p\ell} & \mathbf{Z}_{pp}\end{bmatrix}^{-1} \tag{5}$$

Equation (4) can be written as

$$\mathbf{I}_\ell = \mathbf{Y}_{\ell\ell}\left(\mathbf{V}_{\ell x} - \mathbf{V}_{\ell y}\right)\Delta x - \mathbf{Y}_{\ell p}\mathbf{V}_{py}\Delta x \tag{6}$$

$$0 = \mathbf{Y}_{p\ell}\left(\mathbf{V}_{\ell x} - \mathbf{V}_{\ell y}\right)\Delta x - \mathbf{Y}_{pp}\mathbf{V}_{py}\Delta x \tag{7}$$

From (7), $\mathbf{V}_{py}$ can be calculated as

$$\mathbf{V}_{py} = \mathbf{Y}_{pp}^{-1}\mathbf{Y}_{p\ell}\left(\mathbf{V}_{\ell x} - \mathbf{V}_{\ell y}\right)\Delta x \tag{8}$$

By substituting $\mathbf{V}_{py}$ in (6), $\mathbf{I}_\ell$ can be obtained as

$$\mathbf{I}_\ell = \left(\mathbf{Y}_{\ell\ell} - \mathbf{Y}_{\ell p}\mathbf{Y}_{pp}^{-1}\mathbf{Y}_{p\ell}\right)\left(\mathbf{V}_{\ell x} - \mathbf{V}_{\ell y}\right)\Delta x \tag{9}$$

The induced voltage in the victim conductor in this case is given by (8). It is important to note that in (3), the induced voltage only depends on the mutual impedances between the victim conductor and the phase conductors. In (8), however, all the impedances play a role in calculating the induced voltage in the victim conductor.

The induced voltage is a function of the relative positions of the a-b-c phases and the phasing arrangements. The relative positions vary for different line configurations considered in this paper. Numerical analysis was conducted to find the optimal phase energization for each line design.

III. Test Cases and Simulation Conditions

The test case includes two parallel three-phase transmission lines adjacent to a hypothetical parallel conductor over a 10 km corridor with the geometries and information given in Fig. 2. Conductors are untransposed and bundled. For simplicity, the sagging of conductors is neglected and the victim conductor is considered with the same conductor as for the transmission lines.

For the energization using current source, phase conductors are connected to symmetrical current sources

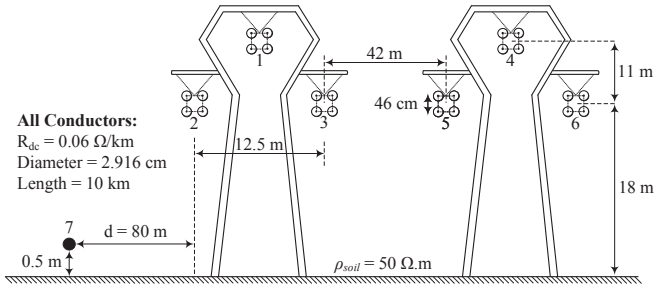

Fig. 2. Two parallel delta transmission lines and a nearby victim conductor.

TABLE I
Different Energizations for Two Parallel Transmission Lines.

Arrangement	Conductors						Arrangement	Conductors					
	1	2	3	4	5	6		1	2	3	4	5	6
I	A	B	C	A	B	C	VII	A	B	C	A	C	B
	B	C	A	B	C	A		C	A	B	C	B	A
	C	A	B	C	A	B		B	C	A	B	A	C
II	A	B	C	B	C	A	VIII	A	B	C	B	A	C
	B	C	A	C	A	B		B	C	A	C	B	A
	C	A	B	A	B	C		C	A	B	A	C	B
III	A	B	C	C	A	B	IX	A	B	C	C	B	A
	B	C	A	A	B	C		B	C	A	A	C	B
	C	A	B	B	C	A		C	A	B	B	A	C
IV	A	C	B	A	C	B	X	A	C	B	A	B	C
	B	A	C	B	A	C		B	A	C	B	C	A
	C	B	A	C	B	A		C	B	A	C	A	B
V	A	C	B	B	A	C	XI	A	C	B	B	C	A
	B	A	C	C	B	A		B	A	C	C	A	B
	C	B	A	A	C	B		C	B	A	A	B	C
VI	A	C	B	C	B	A	XII	A	C	B	C	A	B
	B	A	C	A	C	B		B	A	C	A	B	C
	C	B	A	B	A	C		C	B	A	B	C	A

$(0°, -120°, +120°)$ with the RMS value of 1000 A at the sending-end. To ensure that symmetrical currents flow throughout the conductors, the same currents, as injected to the sending-end, are absorbed at the receiving-end.

Voltage source energization is implemented with RMS values of 525 kV (1.05 pu). The angles of symmetrical voltage source δ at the sending-end are determined using power flow solution. The angle δ is determined such that the average of branch currents equals 1000 A (similar to source current energization). In this case, δ is calculated as 0.5915 degrees.

For a 6-conductor transmission line, there are 36 phase arrangements for energization as indicated in Table I. From these 36 arrangements, only 12 of them are distinct and the rest are variant phase rotations. Table I-left shows arrangements that the rotation of the phases in both circuits is in one direction whereas in Table I-right, rotation of the phases in both circuits is in the opposite direction.

IV. Numerical Results

This section presents the induced voltages obtained with VDE for the test case of Fig. 2.

Figure 3 compares the results for energization using current source and voltage source for different phase arrangements shown in Table I.

As can be seen in Fig. 3, different energization conditions result in different induced voltages. The top ranks for different phase arrangements to obtain the minimum induced voltages are: 7, 10, and 3 for the current source energization, and

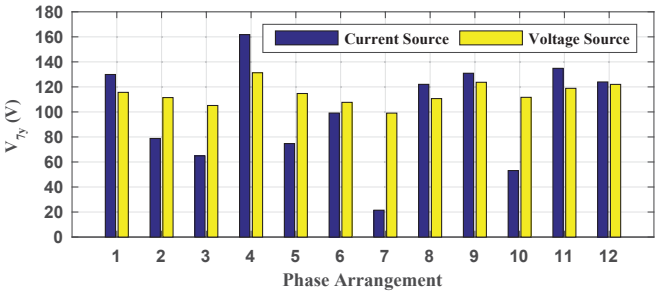

Fig. 3. Induced voltages for different phase arrangement of Fig. 2.

TABLE II
IMPEDANCE MATRIX **Z** CALCULATED AT 60 HZ FOR THE TEST OF FIG. 2.

Resistance Matrix **R** (Ω/km)						
0.06951						
0.05473	0.07139					
0.05473	0.05566	0.07139				
0.05337	0.05414	0.05435	0.06951			
0.05435	0.05516	0.05537	0.05473	0.07139		
0.05414	0.05491	0.05516	0.05473	0.05566	0.07139	
0.05496	0.05604	0.05567	0.05319	0.05421	0.05372	0.07481
Reactance Matrix X (Ω/km)						
0.61034						
0.29615	0.60807					
0.29615	0.29593	0.60807				
0.18734	0.17686	0.19345	0.61034			
0.19345	0.18508	0.20465	0.29615	0.60807		
0.17686	0.16961	0.18508	0.29615	0.29593	0.60807	
0.14617	0.15277	0.14240	0.11242	0.11548	0.10911	0.60433

7, 3, and 6 for the voltage source energization. For both energization conditions, phase arrangement 7 resulted in the minimum induced voltages with 21.5 V for the current source and 99 V for the voltage source.

To understand the reason for such discrepancies between the current source and voltage source energizations in Fig. 3, let us observe the impedance matrix **Z** as an important element for obtaining the induced voltages in (1)–(9). Table II shows the real and imaginary parts of the **Z** matrix obtained at 60 Hz from the Line Constant Routine in the EMTP [15].

Results in Table II indicate that the diagonal elements in the **R** matrix and the diagonal elements in the **X** matrix are similar. Also the off-diagonal elements in the **R** matrix are similar, since there is only one ground return path for all the conductors in Fig. 2 (even though the configuration is highly asymmetrical) [16]. Therefore, matrix of **R** and the diagonal elements of **X** do not make the **Z** matrix unbalance.

On the other hand, the off-diagonal elements of the **X** matrix vary from 0.11 to 0.3 Ω/km. These unbalanced elements of the **Z** matrix make the branch currents unbalance, even though conductors were fed via symmetrical voltage sources. The induced voltage is a result of phase currents multiplied by the respective mutual impedances, as given by (3). For fixed $\mathbf{Z}_{p\ell}$, phase current variations can result in different $\mathbf{V}_{py}$, which explains the differences between the two energization conditions shown in Fig. 3.

In order to define a measure for the level of unbalance in branch currents, the standard deviation for the current amplitudes and phase angle differences with respect to 120° is used,

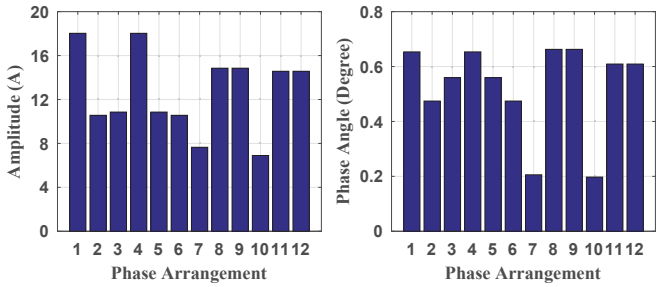

Fig. 4. Standard deviation for the amplitude and phase angle differences of branch currents for the voltage source energization of Fig. 2.

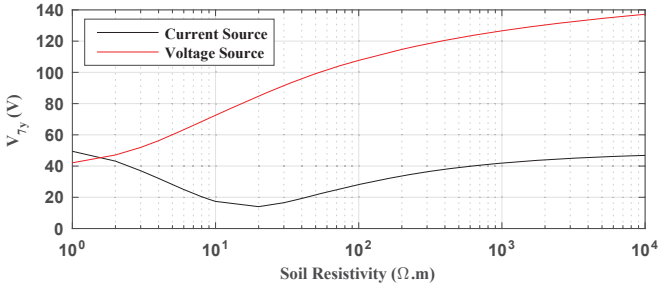

Fig. 5. Sensitivity of the induced voltage to the soil resistivity for the phase arrangement 7 in the test of Fig. 2.

$$SD = \sqrt{\frac{1}{n}\sum_{n}(x_n - x_{ave})^2} \tag{10}$$

In (10), x_{ave} is the average value of the amplitude or phase angle. Figure 4 shows the standard deviation for the amplitudes and the phase angle differences of the branch currents for the voltage source energization in the test of Fig. 2.

As can be observed in Fig. 4, the unbalance of branch currents appears as 7 to 18 A deviation of the amplitudes and 0.2° to 0.65° deviation of phase angle differences. Among different arrangements in Table I, phase arrangements 7 and 10 have the lowest rate of unbalance.

The sensitivity of the induced voltages to the variation of soil resistivity, separation distance of the victim conductor, and different line configurations are studied in the following.

A. Sensitivity to Soil Resistivity

This test is performed by changing the soil resistivity from 1 to 10,000 Ω.m for the phase arrangement 7. This arrangement resulted in the minimum induced voltage in the test case of Fig. 2.

Figure 5 compares the results for the energization using current source and voltage source. These results show that variation of induced voltages is about 35 V for the current source energization and about 100 V for the voltage source energization over the studied soil resistivity range. The discrepancies for the induced voltage obtained with different energization conditions can be as large as 90 to 100 V for soil resistivity values larger than 100 Ω.m. This emphasizes the importance of correct soil characteristic to be used in the simulation when AC interference is of concern.

B. Sensitivity to Separation Distance of Victim Conductor

In this test, the victim conductor is initially located in the middle of the two circuits in Fig. 2. The location of the victim

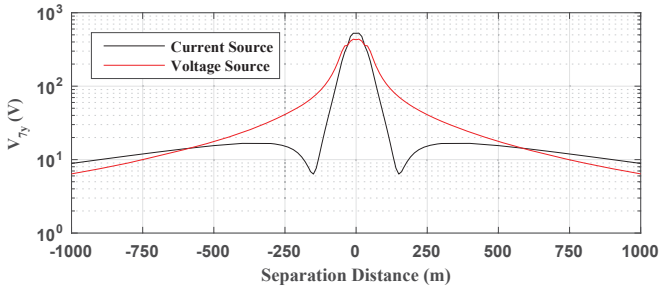

Fig. 6. Sensitivity of the induced voltage to the separation distance of the victim conductor for arrangement 7 in the test of Fig. 2.

conductor is then moved away from the lines up to 1000 m. Sensitivity of the induced voltage to the separation distance is compared in Fig. 6 for the phase arrangement 7.

Figure 6 shows that by increasing the separation distance from 0 to 1000 m, the induced voltage significantly decreases from 436 V to 6 V. The maximum difference between the two energization conditions happens at 150 m where the induced voltage is 6.35 V for the current source energization and 71.6 V for the voltage source energization. The two energization conditions gave similar results for the separation distance equals 30 m (less than 1% error for 360 V).

C. Sensitivity to Different Line Configurations

In this section, the impact of different transmission line configurations on the AC interference levels is assessed. The three line configurations are taken from [17] which include two parallel horizontal lines (Fig. 7a) and double-circuit delta lines in one tower (Figs. 7b and 7c). These lines are located at the left hand-side of the ROW and, similar to Fig. 2, the victim conductor is placed 80 m away from conductor 2. The simulation set up is similar to Fig. 2, except bundled conductors are depicted using a conductor with an equivalent radius in Fig. 7. Simulation results for current source and voltage source energizations are presented in Fig. 8.

As can be observed in Fig. 8, the minimum induced voltage belongs to the double-circuit delta configuration of Fig. 7b. The maximum value for the induced voltage for this configuration is about 80 V for the phase arrangement 12 which is about 100% less than delta configurations of Figs. 2 and 7c and about 200% less than flat configuration of Fig. 7a. The minimum induced voltage for the lines of Fig. 7b is about 8 V for the phase arrangement 6 and for the voltage source energization.

Using double-circuit lines (Figs. 7b and 7c) has an advantage over two parallel lines (Fig. 7a) in terms of the required ROW (cost savings for acquiring land). The electromagnetic interference is also smaller for the double-circuit lines. However, a double-circuit arrangement has lower reliability in comparison with the two parallel lines. This is the main reason for most utilities to choose two parallel lines over a double-circuit arrangement for critical transmission corridors.

The horizontal configuration of Fig. 7a has the highest rate of induced voltages for all the arrangements. The maximum differences for the induced voltage for two parallel configurations (Fig. 2 versus Fig. 7a) were: 140 V for the phase arrangement 1 and for the current source energization, and

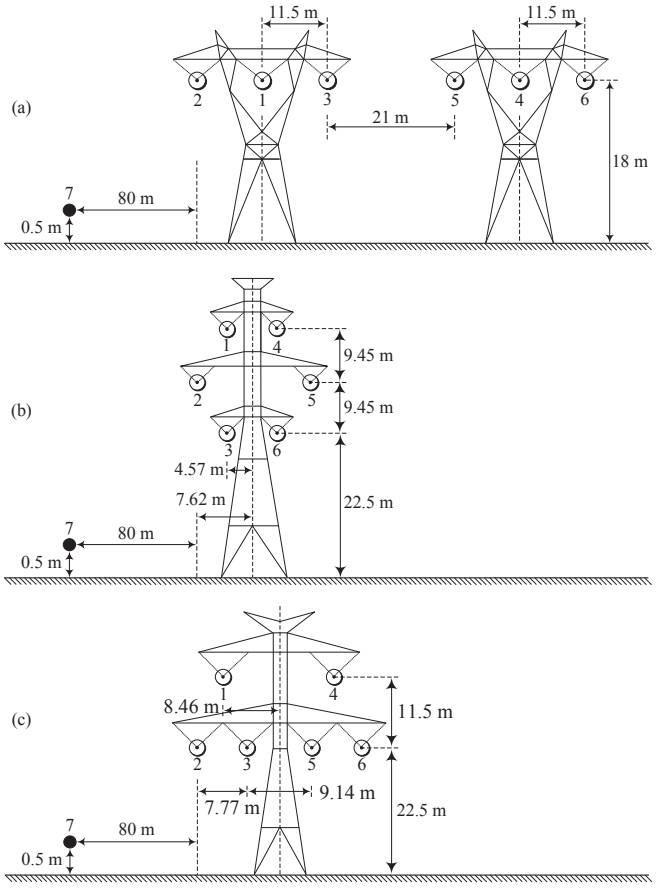

Fig. 7. Different transmission line configurations, a) Two parallel horizontal lines, b) Double-circuit delta lines, c) Double-circuit delta lines.

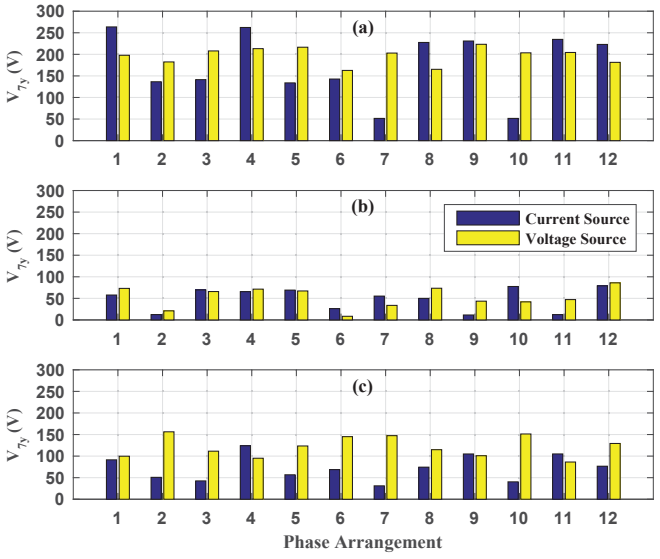

Fig. 8. Sensitivity of the induced voltage to the configuration of the transmission lines of Fig. 7.

104 V for the phase arrangement 7 and for the voltage source energization. These results were used in BC Hydro to choose the delta configuration over the flat configuration.

D. Comparison of Various Simulation Tools

In this section, the induced voltages obtained with VDE are compared with the EMTP simulation using the ULM and the DTFS.

TABLE III
COMPARISON OF VDE, DTFS, AND ULM FOR THE CALCULATION OF THE INDUCED VOLTAGE FOR CURRENT SOURCE ENERGIZATION.

Configuration	Test	VDE	DTFS	ULM
Delta lines (Fig.2)	$\rho = 100\ \Omega.m$	28.16	28.18	27.74
Delta lines (Fig.2)	$d = 200\ m$	11.84	11.84	11.80
Delta lines (Fig.2)	Phase arrangement 3	64.89	64.92	64.81
Horizontal lines (Fig.7a)	Phase arrangement 2	136.50	136.55	136.43
Double-circuit lines (Fig.7b)	Phase arrangement 2	12.35	12.38	11.94
Double-circuit lines (Fig.7c)	Phase arrangement 7	31.12	31.18	31.04

TABLE IV
COMPARISON OF VDE, DTFS, AND ULM FOR THE CALCULATION OF THE INDUCED VOLTAGE FOR VOLTAGE SOURCE ENERGIZATION.

Configuration	Test	VDE	DTFS	ULM
Delta lines (Fig.2)	$\rho = 1000\ \Omega.m$	126.60	127.27	127.40
Delta lines (Fig.2)	$d = 100\ m$	116.01	116.41	116.75
Delta lines (Fig.2)	Phase arrangement 2	111.50	112.15	112.08
Horizontal lines (Fig.7a)	Phase arrangement 12	181.40	182.38	183.12
Double-circuit lines (Fig.7b)	Phase arrangement 6	8.47	8.46	8.63
Double-circuit lines (Fig.7c)	Phase arrangement 9	100.90	101.27	101.62

The steady-state condition for the EMTP was taken at $t = 0.3$ s. For the curve-fitting processes of ULM, the maximum number of poles was set to 35, and the frequency range was set from 10^{-2} to 10^{7} Hz with 10 points per decade. For the DTFS, regular sampling was used for all test cases and no windowing function is needed. The time window width T_c was taken as 4.0 s and the frequency window width f_c was taken as 25 kHz.

Tables III and IV compare the results of different tools for the test conditions in Sections IV-A to IV-C. For each test, the results with the maximum difference are selected, when VDE was taken as reference.

The results in Tables III and IV show that the induced voltages obtained with different tools are very close. Taking the VDE as reference, the maximum error for the DTFS is 0.58% and for the ULM is 3.3%. These errors occur for the phase arrangement 2 for the following tests: Fig. 2 using voltage source for the DTFS and Fig. 7b using current source for the ULM.

V. CONCLUSION

In this paper, we investigated the effect of phase arrangement to minimize the AC interference from two parallel transmission lines to an adjacent hypothetical conductor. It was observed that energization using voltage sources is more realistic than energization using current sources for the simulation of asymmetrical configurations. The inherent unbalance of line impedance creates unbalance phase currents, which reduces the cancellation effect compared to balanced phase currents.

The maximum differences for the induced voltages calculated using two energization conditions was observed to reach about 400% for the phase arrangement 7 (21.5 V for current sources and 99 V for voltage sources). With the optimal phasing for the voltage source energization the induced voltage was reduced by from 131.3 V to 99 V (more than 30%) for the system of two parallel delta lines.

Simulation results showed that variation of soil resistivity from 1 to 300 Ω.m results in increasing the induced voltage form 70 to 140 V (200%) for phase arrangement 7.

Transmission line design is an important factor for minimizing the AC interference. Double-circuit configuration causes lower induced voltages than two parallel lines. In order to minimize the AC interference, delta design was selected over the horizontal design for the proposed 500 kV lines.

The Electro-Magnetic Transients simulation was used to verify the numerical analysis. Comparisons show that the results obtained with Voltage Drop Equations matched with the results of the Universal Line Model and the Discrete-Time Fourier Series.

Further research is required to analyze AC interference for buried conductors, such as pipelines and underground cables.

REFERENCES

[1] K. Kopsidas and I. Cotton, "Induced voltages on long aerial and buried pipelines due to transmission line transients," *IEEE Trans. Power Del.*, vol. 23, no. 3, pp. 1535–1543, Jul. 2008.

[2] D. Markovic, V. Smith, S. Perera, and S. Elphich, "Modelling of the interaction between gas pipelines and power transmission lines in shared corridors," in *Australasian Universities Power Engineering Conference (AUPEC 2004)*, 26–29 Sep. 2004, Brisbane, Australia, pp. 1–6.

[3] R. D. Southey, F. P. Dawalibi, and W. Vukonich, "Recent advances in the mitigation of AC voltages occurring in pipelines located close to electric transmission lines," *IEEE Trans. Power Del.*, vol. 9, no. 2, pp. 1090–1097, Apr. 1994.

[4] L. Šroubová, R. Hamar, and P. Kropík, "Arrangement of phases of double-circuit three-phase overhead power lines and its influence on buried parallel equipment," *Trans. Elect. Eng.*, vol. 4, no. 3, pp. 80–85, 2015.

[5] J. Ma, S. Fortin, and F. P. Dawalibi, "Analysis and mitigation of current unbalance due to induction in heavily loaded multicircuit power lines," *IEEE Trans. Power Del.*, vol. 19, no. 3, pp. 1378–1383, Jul. 2004.

[6] F. P. Dawalibi and R. D. Southey, "Analysis of electrical interference from power lines to gas pipelines. i. computation methods," *IEEE Trans. Power Del.*, vol. 4, no. 3, pp. 1840–1846, Jul. 1989.

[7] F. P. Dawalibi and R. D. Southey, "Analysis of electrical interference from power lines to gas pipelines. ii. parametric analysis," *IEEE Trans. Power Del.*, vol. 5, no. 1, pp. 415–421, Jan. 1990.

[8] L. Grcev and F. P. Dawalibi, "An electromagnetic model for transients in grounding systems," *IEEE Trans. Power Del.*, vol. 5, no. 4, pp. 1773–1781, Oct. 1990.

[9] G. M. Amer, "Novel technique to calculate the effect of electromagnetic field of HVTL on the metallic pipelines by using EMTP program," in *18th Int. Conf. Exhib. Electricity Distribution (CIRED 2005)*, 6–9 Jun. 2005, Turin, Italy.

[10] G. D. Peppas, M.-P. Papagiannis, S. Koulouridis, and E. C. Pyrgioti, "Induced voltage on a above-ground natural gas/oil pipeline due to lightning strike on a transmission line," in *Int. Conf. Lightning Protection (ICLP 2014)*, 11–18 Oct. 2014, Shanghai, China, pp. 461–467.

[11] A. Tavighi, J. R. Martí, and J. A. Gutierrez-Robles, "Comparison of the fdLine and ULM frequency-dependent EMTP line models with a reference laplace solution," *Proc. Int. Conf. on Power Systems Transients (IPST 2015)*, pp. 1–8, Cavtat, Croatia, 15–18 June 2015.

[12] A. Morched, B. Gustavsen, and M. Tartibi, "A universal model for accurate calculation of electromagnetic transients on overhead lines and underground cables," *IEEE Trans. Power Del.*, vol. 14, no. 3, pp. 1032–1038, Jul. 1999.

[13] A. Tavighi, J. R. Martí, V. A. Galván, and J. A. Gutierrez-Robles, "Time-Window-Based Discrete-Time Fourier Series for electromagnetic transients in power systems," *IEEE Trans. Power Del.*, 2018.

[14] J. R. Carson, "Wave propagation in overhead wires with ground return," *Bell Labs Technical Journal*, vol. 5, no. 4, pp. 539–554, Oct. 1926.

[15] H. W. Dommel, *Electromagnetic Transients Program (EMTP) Theory Book*. MicroTran Power System Analysis Corporation, Vancouver, BC, Canada, Sep. 1992.

[16] J. R. Martí and A. Tavighi, "Frequency-dependent multiconductor transmission line model with collocated voltage and current propagation," *IEEE Trans. Power Del.*, vol. 33, no. 1, pp. 71–81, Feb. 2018.

[17] Electric Power Research Institute (EPRI), *Transmission Line Reference Book. 345 kV and above*. 2nd Edition, Boston, MA, USA: General Electric Co., 1982.